Soft Contact Lens With Embedded Moiré Patterns-Based Intraocular Pressure Sensors

Xiaoke Ding, Mingze Chen, Xiaogan Liang, *Member, IEEE*, and Long Que, *Member, IEEE*

***Abstract*— Soft contact lenses with built-in sensors have shown great potential for real-time monitoring of intraocular pressure (IOP). This paper reports a contact lens IOP sensor based on the moiré patterns. One concentric ring grating (G1) is fabricated on a *commercial* contact lens, the other line grating (G2) is stored in a computer. Images of G1 are captured using a smartphone camera. Then moiré patterns are generated by superimposing the images of the two gratings in a computer. The central angle θ formed between two innermost adjacent moiré patterns is extracted as the IOP transducing signals. The performance of the sensor has been evaluated using a home-made hollow hemispherical silicone model eye. The sensitivity of the contact lens IOP sensor is ∼0.15°/mmHg with high repeatability. Additionally, the sensor sensitivity is essentially independent of the initial IOP exerted on the contact lens. Furthermore, the virtual G2 provides great flexibility for the design and fabrication of the sensor, the fabrication of G1 directly on commercial contact lenses paves the way for clinic use. All these results indicate the suitability of this type of sensor for monitoring IOP. [2022-0111]**

***Index Terms*— Contact lens, wearable strain sensor, intraocular pressure, moiré patterns, feature extraction.**

I. Introduction

ELEVATED intraocular pressure (IOP) is a primary contributing factor to glaucoma; its measurement is used for diagnosis of the disease and monitoring the response to therapy [1], [2]. IOP fluctuates significantly such that occasional IOP measurements in the clinician's office are not always sufficient for glaucoma management [3], [4]. Similarly, the IOP of a glaucoma patient who is perceived as well controlled with anti-glaucoma medications may spike between medical visits. Hence, continuous/frequent or real-time IOP monitoring in glaucoma patients is critically needed. To address these issues, a variety of IOP sensors have been reported for potentially continuous monitoring IOP based on different sensing mechanisms [5], [6], [7]. One promising category is the IOP sensors fabricated on the contact lens [8]. After the contact lens is mounted on the cornea, during the IOP fluctuation, it will be deformed along with the eye accordingly. To capture the deformation, different contact lens IOP sensors based on various working principles enabled by microfluidic network [9], [10], photonic crystal [11], nanopore thin film [12], LC resonator [13], [14], resistance [15], [16], and image-processing [9], [10], [17], [18] have been reported. Recently, a 2-D strain sensor based on moiré patterns and image processing algorithms has been reported [19]. Some drawbacks exist for these reported smart contact lenses including negative effects on the retina, cornea, and other ocular systems [20].

Herein, an IOP sensor embedded in a contact lens using the moiré pattern as the transducing signal is reported. Compared to the reported approaches, the moiré patterns-enabled IOP sensor has some considerable advantages including no electromagnetic radiation, no heating issues, power-free, low cost, flexibility of the design and optimization of the virtual grating, and convenient readout through simple imaging. This contact lens IOP sensor (**Figure 1**) has the following features: one concentric ring grating (G1) is fabricated on a commercial contact lens. The other line grating (G2) is stored in a computer. Images of G1 are taken using a smartphone camera and subsequently transferred to a computer. Moiré patterns are then generated by superimposing the images of these two gratings in a computer [20], [21]. Finally, the feature extraction of the moiré patterns is performed using an image processing algorithm [19], [23]. The central angle θ between two *innermost* adjacent moiré fringes in **Figure 1(a)** is extracted as the transducing signals. Due to the corneal curvature's change under different IOP, the curvature of the contact lens changes accordingly, thereby stretching or compressing the contact lens, resulting in the change of the pitch of G1. The moiré patterns in **Figure 1(b)** are expected to change when the contact lens is under tensile strain/pressure or compressive strain/pressure from those under the neutral status accordingly.

II. Materials and Methods

A. Materials and Instruments

Polydimethylsiloxane (PDMS) and its curing agent were purchased from Dow Corning, Midland, Michigan. Contact lenses (with standard solution) were purchased from Johnson & Johnson Vision Care, Inc., Jacksonville, FL. Deionized (DI) water was obtained from a DI water purification system (Millipore, FRANCE). Chrome steel balls were purchased from Global Precision Ball and Roller, New Milford,

Manuscript received 12 June 2022; revised 27 August 2022; accepted 12 September 2022. Date of publication 26 September 2022; date of current version 1 December 2022. This work was supported in part by the National Science Foundation (NSF) at the University of Michigan-Ann Arbor and the Exploratory Research Program at Iowa State University under Award CMMI-2001036. Subject Editor E. Meng. *(Xiaoke Ding and Mingze Chen contributed equally to this work.) (Corresponding authors: Xiaogan Liang; Long Que.)*

Xiaoke Ding and Long Que are with the Department of Electrical and Computer Engineering, Iowa State University, Ames, IA 50011 USA (e-mail: lque@iastate.edu).

Mingze Chen and Xiaogan Liang are with the Department of Mechanical Engineering, University of Michigan, Ann Arbor, MI 48109 USA (e-mail: xiaoganl@umich.edu).

Color versions of one or more figures in this article are available at https://doi.org/10.1109/JMEMS.2022.3206712.

Digital Object Identifier 10.1109/JMEMS.2022.3206712

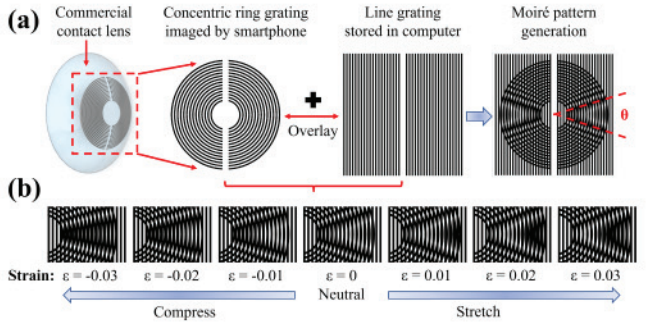

Fig. 1. Moiré patterns-based soft contact lens for IOP sensing. (a) Schematic illustration of the contact lens IOP sensor and its operational principle. (b) Some representative moiré patterns when the contact lens under neutral, tensile and compressive strain, respectively.

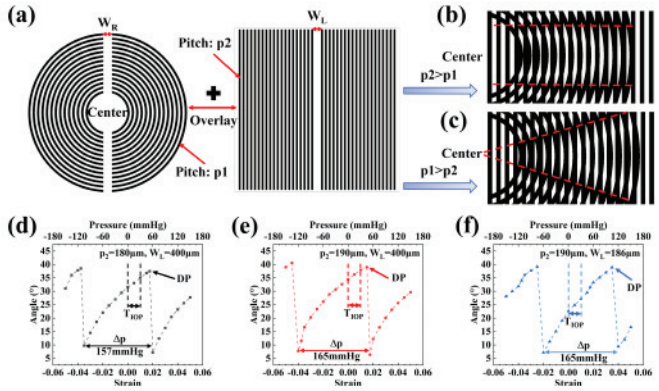

Fig. 2. Design and modeling of the contact lens IOP sensors. (a) Schematic illustration of the main dimensions of the concentric ring grating on contact lens and the virtual line grating; (b–c) Two representative moiré patterns of different shapes and directions with different p1 and p2; (d–f) Simulated results showing different Δp range due to different p2 and W_L, while p1=200 μm for all three designs. For the labels in (d–f): T_{IOP} stands for the target IOP range; DP stands for the discontinuity point.

Connecticut. The pressure gauge was purchased from Fisher Scientific, Pittsburgh, Pennsylvania. Syringe pumps were purchased from Harvard Apparatus, Holliston, Massachusetts.

B. Design and Modeling of the Contact Lens IOP Sensors

Given the periodic nature of the gratings (**Figure 2(a)**), the moiré patterns also change periodically when these two gratings move relative to each other due to the IOP change [24]. For G1, the initial gap sizes between the adjacent grating-lines under the neutral condition are the same. Such gaps change under the applied strain, but it is reasonable to assume they remain the same to each other. Since 21 mmHg is regarded as the threshold value for glaucoma [25], the target detection range of the sensor is from 0 to 30 mmHg, which is the clinic relevant IOP range. Additional design specifications are described as follows. (i) To facilitate the feature extraction from the moiré patterns, careful selection of the pitch (line/gap) sizes of G1 and G2 is needed since their sizes are related to the shape and direction of moiré patterns. By overlaying *virtual* G1 (pitch p1 = 190 μm) and *virtual* G2 (p2 = 200 μm) in a computer, the apex of the angle θ does not converge toward the center of G1 (**Figure 2(b)**). In contrast, when p1=200 μm and p2=190 μm, the angle θ with an apex at the center of G1 is formed (**Figure 2(c)**). In other words, when p1 > p2, the apex of the angle θ converges to the center of the ring grating G1, which facilitates the feature extraction of the patterns. In our designs, p1 > p2 is used as one guideline for designing G1 and G2. (ii) Attention should also be paid to selecting p2 and W_L of G2 in **Figure 2(a)** for optimizing the detection dynamic range and sensitivity of the sensors. To this end, the behaviors and performance of the sensors are further investigated by simulations. The p1 is 200 μm. The behaviors of the moiré fringes by changing p2 and W_L with the IOPs ranging from 0 to 30 mmHg, the target IOP range (T_{IOP}) for the sensors, are summarized in **Figure 2(d-f)**. Given the periodic nature of moiré patterns, the extracted angle θ may not be monotonically continuous in the target IOP range. This behavior is not convenient for IOP quantification since one angle θ may correspond to two IOP values. As such, a wider detection dynamic range can be optimized by tuning the p2. As shown in **Figure 2(d-e)**, the detection dynamic range **Δp** is 157 mmHg when p2 is 180 μm, and the **Δp** is 165 mmHg when p2 is 190 μm. Furthermore, if p2/W_L of G2 are 190 μm/400 μm, when the IOP reaches 45 mmHg, the angle θ drops abruptly from 40.0° to 6.4° at the discontinuity point (**DP**) in **Figure 2(e)**, and then increases again as IOP increases. In contrast, when p2/W_L are 190 μm/186 μm in **Figure 2(f)**, such discontinuity occurs when IOP reaches ~120 mmHg. The angle θ changes continuously in the range of 0-30 mmHg with a much better linearity and larger margin. To facilitate the microfabrication and the image capture of G1, p1 is selected to be 200 μm. As a demonstration, the parameters of G1 and G2 are selected as p1= 200 μm, p2= 190 μm and W_L = 186 μm.

C. Fabrication of the Contact Lens IOP Sensors

To enable scalable fabrication of microstructures on curved and hydrated contact lenses (Johnson & Johnson, Inc.), we implement a shadow-mask-assisted flattening and deposition (SMAFD) method. **Figure 3(a-f)** illustrates the key steps of the SMAFD processes. First, a hydrated contact lens is placed on top of a 3D-printed sample holder. The lens is properly centered to the truncated-cone feature on the holder when its edge is well aligned with the bottom edge of the holding cone (**Figure 3 (a)**). The central region of the lens can be conformally flattened on the holder through pumping away the trapped air in the lens (**Figure 3(b)**). Afterwards, a silicon-based shadow mask bearing concentric ring features is applied on top of the contact lens and aligned with the flattened region of the lens through aligning the holes on the shadow mask with the protrusive pillars on the lens holder (**Figure 3(c)**). This shadow mask is fabricated by using photolithography followed by deep reactive iron etching. After a drying process, the dehydrated contact lens sandwiched by the shadow mask and the sample holder is loaded in an electron-beam evaporator (Enerjet Evaporator) and deposited with 30 nm thick Titanium (**Figure 3(d)**). Ti is chosen because of its good adhesion to the contact lens. Additionally, Ti has been widely used for medical devices because of their excellent corrosion resistance and

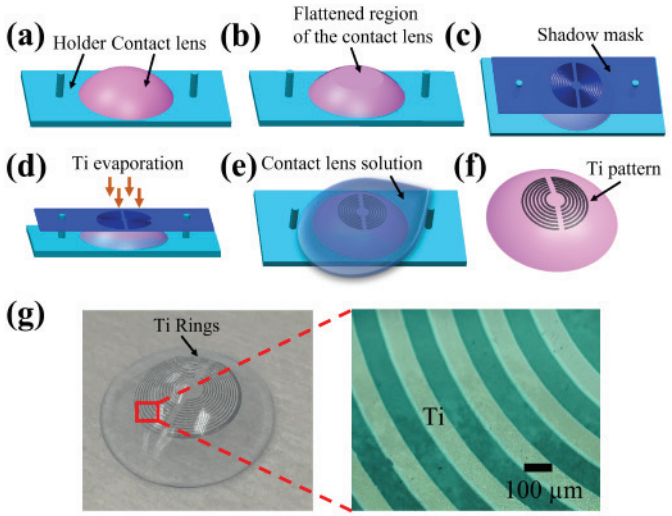

Fig. 3. Fabrication of the contact lens IOP sensors. (a–f) The process flow for fabricating the contact lens IOP sensor; (g) the photo of a fabricated contact lens IOP sensor and its close-up showing the concentric ring grating on the contact lens.

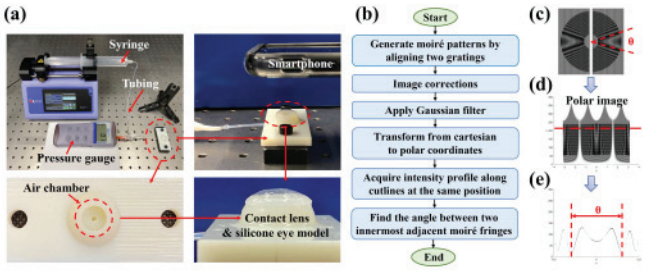

Fig. 4. Experimental setup and image processing procedure. (a) Photo of the setup for evaluating the performance of the IOP sensors. Contact lens attached uniformly on a silicone model eye, which can be deformed by positive or negative pressure from a syringe pump. The images of the concentric ring grating on the contact lens are captured by a smartphone camera, and the pressures applied on the contact lens are monitored by a pressure gauge; (b) The procedure and algorithms for processing the moiré patterns to obtain the relationship between the central angle θ and the applied pressure (i.e., IOP) on the contact lens; (c) Moiré pattern generated by superimposing the image of concentric ring grating and the virtual line grating; (d) Transformed image with polar coordinates; (e) Determination of the angle between two innermost adjacent moiré fringes.

good hard-tissue compatibility [26]. After deposition, the contact lens is soaked into the standard contact lens solution for 5 minutes for re-hydrating the contact lens (**Figure 3(e)**). The Ti deposition is expected to introduce stress and deformation on the hydrogel substrate surface. However, such deposition-induced stress and strain are expected to be very slight because the thickness of deposited Ti (30 nm) is much thinner than that of the substrate (~100 μm). In addition, they can be largely reduced by the re-hydration process. Even if some residual deformation or stretching exists in the contact lens, it does not affect the intraocular pressure measurement using the Ti pattern because the pressure is measured by the relative moiré pattern change between pressurized and initial states of the model eye. Therefore, the residual strain in the contact lens at the initial state is not expected to affect the quantification of the relative moiré pattern change. Finally, the Ti-based grating rings are successfully produced on the curved and hydrate contact lens (**Figure 3(f)**). We expect that the fabrication process introduces sample-to-sample variations in Ti feature sizes and residual strains. However, as aforementioned, the effects of such variations on the final IOP measurements can be effectively minimized through careful calibration of the initial moiré pattern produced by the Ti pattern and quantification of the relative moiré pattern changes. This SMAFD method could be generically implemented to deposit arbitrary functional metal patterns on other curved and flexible hydrogel substrates dedicated to emerging wearable healthcare devices.

Figure 3(g) displays the photograph of a representative contact lens with as-deposited grating rings with a pitch of 200 μm and duty cycle of ~50%. The inner and outer diameters of the whole pattern area are 1.8mm and 7.2mm, respectively, and the pattern consists of 14 rings. The close-up shows an optical micrograph of Ti rings. Our further endurance tests show that the deposited Ti patterns are intact even after days of soaking in contact lens solution.

D. Experimental Setup and Procedure

The setup for the testing of the IOP sensor is shown in **Figure 4(a).** The contact lens is conformally assembled on a home-made hemispherical silicone model eye, which is consequently mounted on a 3D-printed air chamber. Positive or negative pressures are applied to the air chamber through a syringe, which is connected to a syringe pump. As a result, the model eye undergoes deformation, and the pressure on the contact lens can be increased or decreased accordingly. For the hollow hemispherical silicon model eye, its fabrication is summarized as follows [12], [27]. Briefly, polydimethylsiloxane (PDMS, SYLGARD 184 from Dow Corning) is prepared with a volume ratio of 9:1 to curing agent with thorough mixing and degassing for 2 hours. A chrome steel ball is then positioned on a hotplate preheated to 100 °C. The liquid PDMS is poured onto the ball. Liquid PDMS slowly flows down along the surface of the ball and is cured in 3 minutes. Then, a tube with a circular rim is subsequently pressed against the ball to cut through the PDMS, and a silicone model eye with a circular boarder is obtained. The thickness, Young's modulus, and initial radius of curvature of the silicone cornea are ~120 μm, ~0.40 MPa, and 8 mm, respectively, resembling those of the human cornea [28]. The pressure for deforming the contact lens is monitored by a pressure gauge (Fisher Scientific, Inc.). A smartphone camera vertically aligned to the topside of the contact lens is used to record the images of G1 in contact lens and transfers them to a computer. Thereafter a series of moiré patterns are formed by superimposing the G1 images with a corresponding line grating G2. Image processing of these moiré patterns is implemented to extract the angle θ between the two innermost adjacent moiré fringes (**Figure 1**). The procedure and algorithm (**Figure 4(b-e)**) are summarized as follows [19], [23]. The images of moiré patterns are firstly converted into gray scale images, which are subsequently smoothed by a Gaussian low-pass filter to eliminate the grating lines. The processed images are then transformed from Cartesian to polar coordinates. The extracted

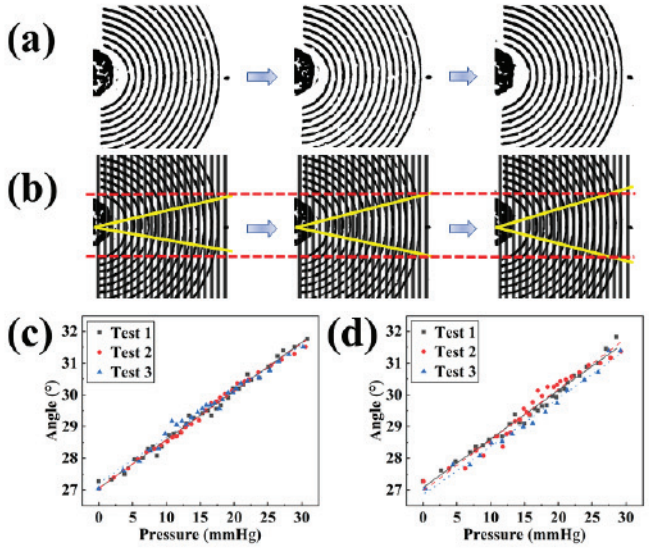

Fig. 5. Representative results of the contact lens IOP sensors. (a) Images of three representative images of concentric ring grating (only part) on the contact lens under different IOPs captured by a smartphone camera; (b) Images of corresponding moiré patterns obtained by overlaying with the virtual line grating; (c) Measured results of the central angle θ vs the IOP for Device-I; (d) Measured results of the central angle θ vs the IOP for Device-II.

angle θ is obtained along a straight *cutline* in **Figure 4(d-e)** from the patterns. As a result, the relationship between the applied IOP and the angle θ can be established.

III. Results and Discussions

The performance of the sensors has been characterized. The measurements of two representative sensors fabricated in the same batch, allowing us to evaluate the fabrication and performance uniformity of the sensors, are reported. (i) **Device-I**: As the IOP changes, the grating p1 on the contact lens could be substantially changed in comparison with its original size. However, it is difficult to observe these changes with the contact lens image alone (**Figure 5(a)**). In contrast, the changes of the angle θ become visible in the moiré patterns (**Figure 5(b)**). The measured result of the angle θ vs the pressure applied on the contact lens demonstrates a clear correlation (**Figure 5(c)**). When the pressure increases by pumping air into the air chamber from 0 to 30 mmHg, the angle θ increases from 27° to 31.5° with high linearity. The results exhibit a high repeatability in triple measurements. The sensitivity of the contact lens IOP sensor is defined as $\Delta\theta/\Delta$IOP, where $\Delta\theta$ refers to the change of the angle θ and ΔIOP stands for the IOP changes. Measurements show that the sensitivity of the sensor is ~0.15°/mmHg. (ii) **Device-II**: The measured results are shown in **Figure 5(d)**. Again, the angle θ shows a linear correlation with the applied pressure with very good repeatability. The sensitivity of this device is ~0.15°/mmHg, consistent with that of the **Device-I**. These results demonstrate (i) the high linear relationship of the angle θ and the IOP with high repeatability, and (ii) the consistence of the developed process for fabricating the sensors. It should be noted that since the silicone eye model is different from the real human eye in terms of its mechanical properties and shape, therefore

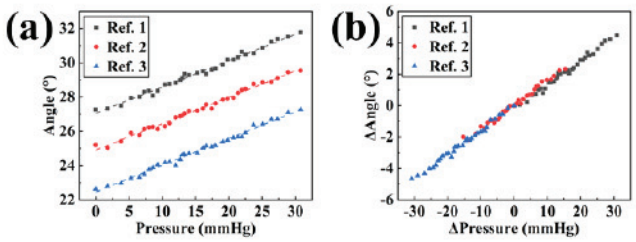

Fig. 6. Representative results of different initial IOPs. (a) Measured results of the central angle θ vs the IOP for Device-I under different initial IOP, Ref. 1 refers to the initial pressure on the device as zero; Ref. 2 refers to the initial pressure on the device as 15 mmHg; Ref. 3 refers to the initial pressure on the device as 30 mmHg; (b) The relationship between $\Delta\theta$ and ΔIOP for these three initial pressures on the contact lens. ΔIOP refers to the IOP change relative to the initial IOP_i: $\Delta IOP = IOP - IOP_i$. $\Delta\theta$ refers to the θ change relative to the θ_i at initial pressure: $\Delta\theta = \theta - \theta_i$.

the measured relationship between the IOP and the angle θ may be different from that for the real eye. However, these measurements can be used to evaluate the performance of the contact lens IOP sensors rapidly before their *in vivo* applications, allowing us to modify their performance quickly by changing the parameters of the IOP sensors such as p1, p2 and W_L.

Due to different anatomy of eyes of different persons, the curvatures of the eyes will be different. When the contact lens is conformally mounted on the eye by a different person, different initial tensile or compress strain on the contact lens could be generated, causing different deformation of the contact lens. Basically, the initial pitch of the G1 in the contact lens could be changed somewhat from the original pitch on the contact lens after being mounted on an eye. Hence it is important to evaluate if the sensitivity of the sensor remains the same or not when the initial pitch of the contact lens is changed. Toward this goal, the following experiments are carried out: (i) measurements of IOPs from 0 to 30 mmHg with an initial pressure on contact lens of 0 mmHg (i.e., neutral status); (ii) measurements of IOPs from 15 to 30 mmHg and from 15 to 0 mmHg with an initial pressure on contact lens of 15 mmHg, and (iii) measurements of IOPs from 30 to 0 mmHg with an initial pressure on the contact lens of 30 mmHg. In other words, the measurements of the responses of an IOP sensor with three representative initial pressures (0, 15 mmHg and 30 mmHg) in a dynamic range ΔIOP from 0 to 30 mmHg are used as the examples. The measured results are summarized in **Figure 6(a)**. All these measurements show that the angle θ and the IOP have a linear relationship with essentially identical slopes, indicating all have the same sensitivity even though the initial pressure on contact lens is different. It should be noted that when other initial pressures applied on the contact lens for the measurements, the similar results can be obtained. Basically, the sensitivity of this type of sensor is independent of the initial pressure applied on the contact lens. By combining these measurements, a plot showing the relationship between $\Delta\theta$ and **ΔIOP** for these initial pressures on the contact lens is given in **Figure 6(b)**, where $\Delta\theta = \theta - \theta_i$ and θ_i is the central angle at the initial pressure; $\Delta IOP = IOP - IOP_i$ and IOP_i is the initial pressure.

For the same IOP sensor, no matter what the initial IOP on the contact lens is, the sensitivity of the sensor remains the same. This feature suggests that for a specific contact lens IOP sensor of this type, as far as we have determined its sensitivity, potentially we do not need calibrate its sensitivity for its use for different patients.

IV. Conclusion

In summary, a moiré patterns-based contact lens IOP sensor has been designed, fabricated and tested. The demonstration of the concentric ring grating (G1) images simply captured by a smartphone camera, and the formation of the moiré patterns between the G1 and the virtual line grating (G2) in a computer indicate the feasibility to develop a new type of contact lens IOP sensors. The moiré patterns and image processing approach are particularly attractive because of the flexibility of design and optimization of the virtual line grating for the targeted detection dynamic range and sensitivity of the IOP sensor. A fabrication process has been developed to fabricate gratings directly on the commercial contact lenses, eliminating the possible barriers for clinic applications of this type of sensor for achieving real-time and continuous monitoring of IOP for glaucoma diagnosis.

References

[1] Y. C. Tham, X. Li, Y. Tien Wong, A. Harry Quigley, T. Aung, and C.-Y. Cheng, "Global prevalence of glaucoma and projections of glaucoma burden through 2040: A systematic review and meta-analysis," *Ophthalmology*, vol. 121, no. 11, pp. 2081–2090, 2014.

[2] A. Heijl, M. C. Leske, B. Bengtsson, L. Hyman, and M. Hussein, "Reduction of intraocular pressure and glaucoma progression," *Evidence-Based Ophthalmol.*, vol. 4, no. 3, pp. 137–139, 2003.

[3] D. Anderson, "Normal-tension glaucoma (low-tension glaucoma)," *Indian J. Ophthalmol.*, vol. 59, no. 7, p. 97, 2011.

[4] N. Farandos, K. A. Yetisen, J. M. Monteiro, R. C. Lowe, and S. H. Yun, "Smart lenses: Contact lens sensors in ocular diagnostics," *Adv. Healthcare Mater.*, vol. 4, no. 6, p. 785, 2015.

[5] J. Fernandes, Y. H. Kwon, J.-J. Kim, H. Liu, and H. Jiang, "High contrast grating based strain sensor for intraocular applications," *J. Microelectromech. Syst.*, vol. 27, no. 4, pp. 599–601, Aug. 2018.

[6] M. Yuan *et al.*, "Electronic contact lens: A platform for wireless health monitoring applications," *Adv. Intell. Syst.*, vol. 2, no. 4, Apr. 2020, Art. no. 1900190.

[7] C. Yang *et al.*, "Wearable and implantable intraocular pressure biosensors: Recent progress and future prospects," *Adv. Sci.*, vol. 8, no. 6, Mar. 2021, Art. no. 2002971.

[8] C. Yang *et al.*, "Intelligent wireless theranostic contact lens for electrical sensing and regulation of intraocular pressure," *Nature Commun.*, vol. 13, no. 1, pp. 1–15, Dec. 2022.

[9] I. E. Araci, B. Su, S. R. Quake, and Y. Mandel, "An implantable microfluidic device for self-monitoring of intraocular pressure," *Nature Med.*, vol. 20, no. 9, pp. 1074–1078, Sep. 2014.

[10] W. Yang *et al.*, "Notched-ring structured microfluidic contact lens for intraocular pressure monitoring," *Appl. Phys. Lett.*, vol. 119, no. 19, Nov. 2021, Art. no. 193701.

[11] B. Maeng, H.-K. Chang, and J. Park, "Photonic crystal-based smart contact lens for continuous intraocular pressure monitoring," *Lab Chip*, vol. 20, no. 10, pp. 1740–1750, 2020.

[12] C. Song, G. Ben-Shlomo, and L. Que, "A multifunctional smart soft contact lens device enabled by nanopore thin film for glaucoma diagnostics and *in situ* drug delivery," *J. Microelectromech. Syst.*, vol. 28, no. 5, pp. 810–816, Oct. 2019.

[13] M. Kouhani, J. Wu, A. Tavakoli, J. A. Weber, and W. Li, "Wireless, passive strain sensor in a doughnut-shaped contact lens for continuous non-invasive self-monitoring of intraocular pressure," *Lab Chip*, vol. 20, no. 2, pp. 332–342, 2020.

[14] K. Mansouri, A. F. Medeiros, A. Tafreshi, and N. Robert Weinreb, "Continuous 24-hour monitoring of intraocular pressure patterns with a contact lens sensor: Safety, tolerability, and reproducibility in patients with glaucoma," *Arch. Ophthalmol.*, vol. 130, no. 12, pp. 1534–1539, 2012.

[15] J. Xu *et al.*, "Highly transparent and sensitive graphene sensors for continuous and non-invasive intraocular pressure monitoring," *ACS Appl. Mater. Interface*, vol. 12, no. 16, pp. 18375–18384, Apr. 2020.

[16] J. Kim *et al.*, "Wearable smart sensor systems integrated on soft contact lenses for wireless ocular diagnostics," *Nature Commun.*, vol. 8, no. 1, pp. 1–8, Apr. 2017.

[17] A. Phan, P. Truong, J. Trumpp, and F. E. Talke, "Design of an optical pressure measurement system for intraocular pressure monitoring," *IEEE Sensors J.*, vol. 18, no. 1, pp. 61–68, Jan. 2018.

[18] S.-H. Lee, K.-S. Shin, J.-W. Kim, J.-Y. Kang, and J.-K. Kim, "Stimulus-responsive contact lens for IOP measurement or temperature-triggered drug release," *Transl. Vis. Sci. Technol.*, vol. 9, no. 4, p. 1, Mar. 2020.

[19] X. Ding and L. Que, "Design, modeling and validation of a flexible strain sensor based on Moire patterns and image processing," in *Proc. 21st Int. Conf. Solid-State Sensors, Actuat. Microsyst. (Transducers)*, Jun. 2021, pp. 1303–1306.

[20] J. A. Elder, "Ocular effects of radiofrequency energy," *Bioelectromagnetics*, vol. 24, no. S6, pp. S148–S161, 2003.

[21] G. Oster, M. Wasserman, and C. Zwerling, "Theoretical interpretation of Moiré patterns," *J. Opt. Soc. Amer.*, vol. 54, no. 2, pp. 169–175, 1964.

[22] M. Abolhassani and M. Mirzaei, "Unification of formulation of Moiré fringe spacing in parametric equation and Fourier analysis methods," *Appl. Opt.*, vol. 46, no. 32, p. 7924, 2007.

[23] P. Y. Tan, M. M. Ratnam, and F. Ahmad, "Feature extraction from Moiré pattern images for tilt sensing," in *Proc. Int. Conf. Imag., Signal Process. Commun. (ICISPC)*, 2017, pp. 24–29.

[24] R. Stevens, "Optical inspection of periodic structures using lens arrays and Moiré magnification," *Imag. Sci. J.*, vol. 47, no. 4, pp. 173–179, 1999.

[25] A. Heijl, "Reduction of intraocular pressure and glaucoma progression: Results from the early manifest glaucoma trial," *Arch. Ophthalmol.*, vol. 120, no. 10, p. 1268, Oct. 2002.

[26] T. Hanawa, "Titanium–tissue interface reaction and its control with surface treatment," *Frontiers Bioeng. Biotechnol.*, vol. 7, p. 170, Jul. 2019.

[27] X. Ding, G. Ben-Shlomo, and L. Que, "Soft contact lens with embedded microtubes for sustained and self-adaptive drug delivery for glaucoma treatment," *ACS Appl. Mater. Interface*, vol. 12, no. 41, pp. 45789–45795, Oct. 2020.

[28] T. Rossi *et al.*, "The pathogenesis of retinal damage in blunt eye trauma: Finite element modeling," *Investigative Opthalmol. Vis. Sci.*, vol. 52, no. 7, p. 3994, Jun. 2011.

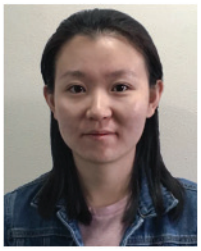

Xiaoke Ding received the B.E. degree in materials engineering from the University of Electronic Science and Technology of China, Chengdu, China, in 2015, and the M.S. degree in materials engineering from the University of Florida, Gainesville, FL, USA, in 2017. She is currently pursuing the Ph.D. degree in electrical engineering with Iowa State University, Ames, IA, USA. Her research interests include developing multifunctional flexible and wearable platforms with anodic aluminum oxide and other micro-nanostructures for biomedical applications, such as intraocular pressure monitoring, drug delivery, and biomarker detection.

Mingze Chen received the B.S. degree in mechanical engineering from the University of Illinois at Urbana-Champaign, Champaign, IL, USA, in 2018. He is currently pursuing the Ph.D. degree in mechanical engineering with the University of Michigan, Ann Arbor, MI, USA. His research interests include fabricating biosensor and photo detector on patterned 2-D layered material and other micro-nanostructures for metrology and biomedical applications.

Xiaogan Liang (Member, IEEE) received the B.S. degree in physics from Peking University, the M.S. degree in condensed matter physics from the Institute of Semiconductors, Chinese Academy of Sciences, and the Ph.D. degree in electrical engineering from Princeton University. He is currently working as an Associate Professor with the Department of Mechanical Engineering, University of Michigan (UM). He has coauthored 72 journal publications and more than 50 conference presentations, has given more than 30 invited presentations, and holds eight U.S. patents. His current research interests are focused on nanofabrication, nanomanufacturing, microsystem integration, nanoelectronics and optoelectronics based on low-dimensional nanostructures, biosensors, and microdrone sensors. He is a member of Sigma Xi and ASME. He was a recipient of the NSF CAREER Award.

Long Que (Member, IEEE) received the bachelor's degree in physics from Peking University, China, and the Ph.D. degree in electrical engineering from the University of Wisconsin–Madison in 2000.

He was a Visiting Scholar with the Center for Wireless Integrated Microsystems, University of Michigan, Ann Arbor, and the Center for Nanoscale Materials, Argonne National Laboratories. Then, he worked with GE-Global Research Center as a Task Leader and a Project Leader, and he was a John Cordaro/Entergy Endowed Associate Professor with Louisiana Tech. He is currently a Professor with the Department of Electrical and Computer Engineering, Iowa State University. He has published three book chapters and over 100 papers in major conferences and journals. He has over 25 awarded and pending U.S. patents. His patents have been used or licensed by companies, such as GE and Intel. His current research interests include bionanotechnology, bioMEMS, renewable energy technologies, nanomaterials, and nanodevices enabled by self-assembly technique. He is a fellow of the International Association of Advanced Materials (IAAM). He received the National Research Award from the Chinese Academy of Sciences in 1997. He won invention awards from GE for over ten U.S. patents. He was a recipient of the NSF-CAREER Award. His research group received the Research Award from Louisiana Tech and the Recognition Award from the Board of Regents of Louisiana in 2009. He also received the Outstanding Invention Award from Louisiana Tech in 2011. His research group received the Best Student Paper Award at IEEE SENSORS Conference 2016.